

Key Points:

- Murchison meteorite samples were irradiated with electrons and laser to model effects of space weathering
- Hydrogen sulfide (H_2S) and hydrogen disulfide (H_2S_2) were generated from sulfur-containing minerals at low temperature
- Conversion of sulfur-containing mineral to volatile H_2S may induce the surficial sulfur depletion on asteroids

Supporting Information:

- Supporting information

Correspondence to:

R. I. Kaiser,
ralfk@hawaii.edu

Citation:

Zhu, C., Góbi, S., Abplanalp, M. J., Frigge, R., Gillis-Davis, J. J., & Kaiser, R. I. (2019). Space weathering-induced formation of hydrogen sulfide (H_2S) and hydrogen disulfide (H_2S_2) in the murchison meteorite. *Journal of Geophysical Research: Planets*, 124, 2772–2779. <https://doi.org/10.1029/2018JE005913>

Received 21 DEC 2018

Accepted 19 SEP 2019

Accepted article online 21 OCT 2019

Published online 6 NOV 2019

Space Weathering-Induced Formation of Hydrogen Sulfide (H_2S) and Hydrogen Disulfide (H_2S_2) in the Murchison Meteorite

Cheng Zhu^{1,2} , Sándor Góbi^{1,2,4} , Matthew J. Abplanalp^{1,2}, Robert Frigge^{1,2} , Jeffrey J. Gillis-Davis³ , and Ralf I. Kaiser^{1,2} 

¹Department of Chemistry, University of Hawai'i at Mānoa, Honolulu, HI, USA, ²W.M. Keck Laboratory in Astrochemistry, University of Hawai'i at Mānoa, Honolulu, HI, USA, ³Hawaii Institute of Geophysics and Planetology, University of Hawai'i at Mānoa, Honolulu, HI, USA, ⁴Present address: CQC, Department of Chemistry, University of Coimbra, Coimbra, Portugal

Abstract Theoretical calculations and experimental simulations indicate that the surprisingly low sulfur abundance on the surfaces of spacecraft visited S-type asteroids 433 Eros and 25143 Itokawa may be due to space weathering. Two current missions, Osiris-Rex and Hayabusa 2, are studying asteroids 101955 Bennu (B-type) and 162173 Ryugu (C-type), respectively. Understanding space weathering effects related to sulfur containing species is only in the beginning stages and has not been studied from the point of view of C-type asteroids. This laboratory study details the formation of hydrogen sulfide (H_2S) and hydrogen disulfide (H_2S_2) from conversion of nonvolatile-sulfuretted species in the Murchison meteorite by exposure to energetic electrons and laser processing, which mimics the synergic effect of secondary electrons generated by galactic cosmic rays and high-energy solar wind particles plus micrometeorite impact on airless bodies. The results indicate that space weathering processes likely induce depletion of sulfur on the surface of C-type and undifferentiated S-type asteroids. For keeping scientific integrity of these fragile species, cold/cryogenic curation of future collected samples from asteroids might be required.

Plain Language Summary The Near Earth Asteroid Rendezvous (NEAR) Shoemaker and Hayabusa spacecraft have detected surprisingly low sulfur abundance on the surfaces of asteroids 433 Eros and 25143 Itokawa. The physical and chemical properties of the surfaces of asteroids are affected by space weathering processes including irradiation by cosmic rays and bombardment of micrometeorites. However, understanding space weathering effects related to sulfur containing species is only in the beginning stages. Here we show that hydrogen sulfide (H_2S) and hydrogen disulfide (H_2S_2) can be generated from conversion of nonvolatile sulfuretted species in the Murchison meteorite by simulated weathering processes. The Murchison meteorite is suggested to originate from asteroids. These volatile sulfur-containing species sublimed at temperatures lower than the maximum surface temperatures (with the Sun overhead) on asteroids. These results indicate that space weathering likely induces depletion of sulfur on the surfaces of asteroids.

1. Introduction

Sulfur depletion has been found at two S-type asteroids—433 Eros and 25143 Itokawa (Keller & Berger, 2014; McCoy et al., 2001; McFadden et al., 2001; Nittler et al., 2001; Trombka et al., 2000). Data taken by the visible-near infrared spectrometer and the X-ray/Gamma-ray Spectrometer on board the Near Earth Asteroid Rendezvous Shoemaker spacecraft indicate that the surface chemistry of Eros is similar to ordinary chondrites (OC; McCoy et al., 2001; McFadden et al., 2001), which is consistent with Earth-based observations (Chapman, 1995; Kelley et al., 2001; Murchie & Pieters, 1996). However, the measured upper limit of the sulfur to silicon weight ratio ($S:Si = 0.05$) on the surface of Eros is significantly lower than ratios of 0.075–0.165 in OC (Nittler et al., 2001). Transmission electron microscope coupled with energy-dispersive X-ray spectroscopy analysis of the particle (RA-QD02-0125) from asteroid 25143 Itokawa returned by the Hayabusa mission identified a pyrrhotite grain with a disordered rim on its surface. The rim was found to be sulfur-depleted by up to 75% with dispersive nanophase iron (Fe) grains on the outermost surface (Keller & Berger, 2014).

Space weathering, composed of a complex set of processes (e.g., galactic cosmic rays (GCR), solar wind particles, and bombardment by micrometeorites), is proposed to be responsible for the low sulfur abundance on

the surface of S-type asteroids (Foley et al., 2006; Gillis-Davis & Scott, 2014; Keller et al., 2013; Killen, 2003; Kracher & Sears, 2005; Loeffler et al., 2008; Nittler et al., 2001; Trombka et al., 2000). Killen (2003) modelled aluminum (Al) projectiles impact onto troilite (FeS)—the primary sulfur-bearing mineral in OC—and enstatite. The results show that the vaporization rate for the sulfur-containing species is nine times as fast as that for the latter refractory species. Laboratory simulations of solar wind irradiation by 4 keV ions and micrometeorite impact by laser pulses (193 nm) on FeS revealed similar decrease of the S:Fe atomic ratio on the surface (up to 2.5) to that of the Near Earth Asteroid Rendezvous measurements (at least 1.5; Loeffler et al., 2008). Keller et al. (2013) reported that 5 keV gallium ions (Ga^+) irradiation of FeS results in preferential sputtering of S and the formation of nanophase Fe. Furthermore, the relative sputtering rate of FeS by energetic Ga^+ was found to be much higher than that of olivine or enstatite. Gillis-Davis and Scott (2014) observed the release of volatile hydrogen sulfide (H_2S) during laser irradiation of Holbrook (L6) OC, which may originate from S-type asteroids like Eros. This result implies that sulfur-containing species on Eros may be converted to H_2S by micrometeorite impact and lost into space. However, S-type asteroids represent only about 30% of the asteroid belt (DeMeo & Carry, 2014). Approximately half of all known asteroids belong to C-complex—where “complex” refers to a range of similar spectral taxonomic classes (e.g., C, B, D, F, and G)—yet the fundamental effects of space weathering on sulfur-containing species on the surfaces of C-complex asteroids are not well known.

Here, we demonstrate that H_2S and hydrogen disulfide (H_2S_2) can form in the Murchison CM2 meteorite upon exposure to energetic electrons and laser processing. These irradiations are intended to mimic the combined effects of secondary electrons generated by GCR and high-energy solar wind particles plus micrometeorite impact on airless bodies; two principal components of the space weathering process. As the link between the CM meteorites and the C-type asteroids has been well established (Burbine, 2014), we suggest that sulfur on the surface of C-type asteroids, and C-complex asteroid in general, may be depleted via generation of volatile H_2S and H_2S_2 by space weathering. Hence, we predict the current C-complex asteroid sample-return missions OSIRIS-REx/NASA (launched in 2016) and Hayabusa 2/JAXA (launched in 2014) would detect sulfur depletion on the surfaces of asteroids 101955 Bennu and 162173 Ryugu, respectively.

2. Experimental

The experiments were conducted in a contamination-free ultra-high vacuum stainless chamber evacuated to a base pressure of a few 10^{-11} Torr exploiting magnetically suspended turbo molecular pumps backed by oil-free scroll pumps (Jones & Kaiser, 2013). Within the chamber, a silver mirror substrate is interfaced to a cold finger via indium foil for thermal conductivity. The cold finger is cooled by a closed-cycle helium compressor (Sumitomo Heavy Industries, RDK-415E) while the temperature can be maintained between 5.5 ± 0.1 K and 300.0 ± 0.1 by the help of a cartridge heater connected to a programmable temperature controller (Lakeshore, Mode 336). The substrate is able to be rotated in the horizontal plane and translated in the vertical plane with the assistance of a doubly differentially pumped rotational feedthrough (Thermionics Vacuum Products, RNN-600/FA/MCO) and an ultra-high vacuum compatible bellow (McAllister, BLT106), respectively.

A $57 \pm 7 \mu\text{m}$ thick layer of Murchison meteorite crushed powder was pressed onto a silver substrate. The mass of the powder was 0.0306 ± 0.0005 g, and the average density of the precrushed meteorite was $2.83 \pm 0.18 \text{ g/cm}^3$ (McCausland et al., 2011). The powder was made by crushing and dry sieving a bulk sample of Murchison to grain size of less than $45 \mu\text{m}$. The Murchison meteorite was provided by Dr. Mike Zolensky, given from his own personal collection. The sample was then cooled to 5.5 ± 0.1 or 150.0 ± 0.1 K whereupon it was irradiated simultaneously by infrared pulsed laser ($10.6 \mu\text{m}$) from a SYNRAD Firestar v40 carbon dioxide (CO_2) laser operated at 14% of full power (pulse width of $30 \mu\text{s}$) and by energetic electrons with an energy of 5 keV from a Specs EQ 22-35 electron gun (Table 1). Infrared μs laser and energetic electron irradiations simulate thermal effects of micrometeorite bombardments (Basilevsky et al., 2000; Hiroi et al., 2003; Moroz et al., 1996; Moroz et al., 2004; Moroz et al., 2009; Shingareva et al., 2004; Wasson et al., 1998), and secondary electrons released during GCR and high-energy solar wind particles penetrating asteroid regoliths (Bennett et al., 2005; Johnson, 1990; Turner et al., 2016), respectively. In the planetary science community, both ns (Brunetto et al., 2007; Gillis-Davis et al., 2017; Hiroi & Sasaki, 2001; Sasaki et al., 2001) and μs (Basilevsky et al., 2000; Hiroi et al., 2003; Moroz et al., 1996; Moroz et al.,

Table 1
Summary of the parameters involved in the space-weathering experiments

	Electron Beam	Laser
Angle of incidence (deg)	70	45
Initial energy of the electrons (keV)	5	
Electron current (μA)	10 ± 1	
Laser power (W/cm^2)		8.0 ± 0.4
Irradiation time (min)	300	300
Average penetration depth (μm)	0.14 ± 0.02	15 ± 3
Dose per atomic mass unit (eV/amu)	150 ± 30	
Total deposited laser energy (J/m^2)		$(1.4 \pm 0.2) \times 10^9$

2004; Moroz et al., 2009; Shingareva et al., 2004; Wasson et al., 1998) lasers are exploited to simulate micrometeorite impacts. The ns laser experiments simulate the initial impact caused shock heating, which results in projectile vaporization and cratering on targets, while the μs laser studies encompass the time scale of thermal dissipation to impact adjacent regions, which may induce thermal diffusion and enhance bond-breaking processes. Our preliminary studies using Fourier-transform infrared spectroscopy and quadrupole mass spectrometry (QMS) found that irradiation of the samples with only energetic electrons or laser does not generate noteworthy new species. The deposited energy of the laser and the irradiation dose of the 5 keV electrons as computed via Monte Carlo simulations (CASINO v2.42; Drouin et al., 2007) are compiled in Table 1. It is important to extrapolate these laboratory simulations to the astrophysical environment.

The particle component of GCR and solar wind mainly consists of protons (H^+) and helium nuclei (He^{2+}) with low energy part ($E \approx 1 \text{ keV}$) and high-energy part ($E \approx 100 \text{ keV}$; Strazzulla & Johnson, 1989). The penetration depth in silicates of a low energy particle ($E \approx 1 \text{ keV}$) is only a few tens of nanometers (Crandall et al., 2017), which is significantly smaller than the impact and subsequent thermal diffusion depth (more than few tens of micrometers) of a typical hypervelocity micrometeorite (Fletcher et al., 2015; Zook et al., 1970). High-energy particles ($E \approx 100 \text{ keV}$) can easily penetrate deeper than micrometer regions and generate significant synergic effects with micrometeorite impacts. Therefore, in this study, we only considered the dose of the high-energy particles ($E \approx 100 \text{ keV}$), which is $10 \text{ eV per } 10^4 \text{ years per small molecule such as methane (CH}_4\text{) at 1 AU}$ (Strazzulla & Johnson, 1989). Investigating effects of low energy solar wind protons is also an interesting topic but out of the scope of this study. If the flux of these particles follows the inverse-square law, the dose in the asteroid belt at 3 AU can be determined to be $6.9 \times 10^{-6} \text{ eV}\cdot\text{amu}\cdot\text{year}$, which is one ninth of that at 1 AU. These high-energy particles lose their energy almost exclusively (99.99%) via electronic interaction to the target molecules and generate secondary electrons with kinetic energies up to a few keV. Energetic electrons have been widely used in the planetary science and astrochemistry communities to simulate these secondary electrons (Abplanalp, Gozem, et al., 2016; Boamah et al., 2014; Boyer et al., 2014; Harris et al., 1995; Shingledecker & Herbst, 2018; Turner et al., 2018). The micrometeorite impact energy in the asteroid belt was estimated to be $\sim 1,000 \text{ J}\cdot\text{m}^2\cdot\text{year}$ as it is about two orders of magnitude (Chapman et al., 1989) higher than that on the Moon ($\sim 10 \text{ J}\cdot\text{m}^2\cdot\text{year}$; Love & Brownlee, 1993; Lucey et al., 2006). Therefore, the laboratory electron-irradiation dose at $150 \pm 30 \text{ eV/amu}$ and laser-irradiation dose at $(1.4 \pm 0.2) \times 10^9 \text{ J/m}^2$ (Table 1) correspond to those received by silicates on asteroid surfaces in 10^6 to 10^7 years. The simulated average penetration depths of the laser of $15 \mu\text{m}$ and of the electrons ($0.14 \pm 0.02 \mu\text{m}$) are both less than the thickness of the sample ($57 \pm 7 \mu\text{m}$), which eliminates any interaction between the laser and electrons with the substrate.

The irradiated samples were kept at $5.5 \pm 0.1 \text{ K}$ or $150.0 \pm 0.10 \text{ K}$ for 1-hr post irradiation and then warmed up to 300 K at a rate of 1 K/min (temperature programmed desorption; TPD). The TPD profiles of the sublimed molecules from the irradiated samples at different temperatures ($5.5 \pm 0.1 \text{ K}$; $150.0 \pm 0.1 \text{ K}$) were collected via photoionization reflectron time-of-flight mass spectrometry (PI-ReTOF-MS). This technique utilizes pulsed coherent vacuum ultraviolet (VUV) light at 118.2 nm (10.49 eV) to ionize the subliming molecules. The ionized molecules were mass analyzed with a ReTOF mass spectrometer (Jordan TOF Products, Inc.) based on the arrival time to a multichannel plate. The signals were then amplified with a fast preamplifier (Ortec 9305) and recorded with a personal computer multichannel scalar (FAST ComTec, P7888-1 E) in 4 ns bin widths, which was triggered via the pulse delay generator at 30 Hz (Quantum Composers 9518). The final mass spectrum is the summation of 3,600 sweeps.

The PI-ReTOF-MS bears two key advantages compared to traditional electron impact ionization mass spectrometry (EI-QMS). First, a typical QMS using an electron impact ionizer operating at 70–100 eV electron energy does not only ionize molecules but also results in a significant fragmentation of the parent ion thus forming numerous fragment ions and even leads to the absence of signal from the molecular parent ion. Our “soft” single photon ionizing source (e.g., 10.49 eV) does not result in fragmentation of the molecular ion, if ionized close to the ionization limit (Abplanalp et al., 2015; Abplanalp, Förstel, & Kaiser, 2016). Second, even though exploiting soft ionization with low-energy electrons of a few eV kinetic energy, the

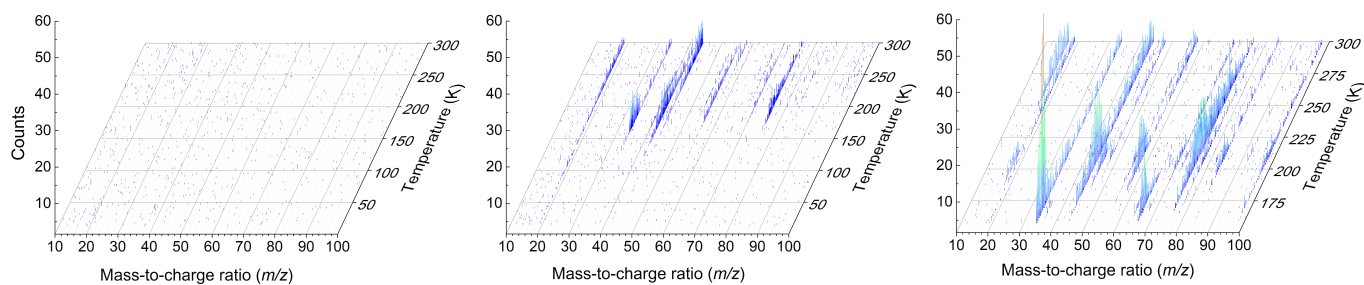


Figure 1. Mass-to-charge dependent temperature programmed desorption (TPD) profiles obtained after photoionizing the desorbing molecules of the Murchison sample at 10.49 eV. (a) blank, (b) electron and carbon dioxide laser exposure at 5.5 K, and (c) electron and carbon dioxide laser exposure at 150 K.

resolution is typically only 1.0 eV, which makes it hard to differentiate species with ionization energies differing less than 1.5 eV. The energy of single photon used in PI-ReTOF-MS can be “controlled” within a resolution of at least 0.01 eV (Abplanalp, Gozem, et al., 2016; Turner et al., 2015).

3. Results

Figure 1 depicts the intensities of the mass-to-charge ratios up to $m/z = 100$ as a function of the temperature during the TPD phase of the unirradiated (blank) and irradiated (5 and 150 K) Murchison samples recorded via highly sensitive PI-ReTOF-MS using 10.49 eV. No signal was detected in the blank experiment (Figure 1a), which confirms that the peaks observed in the irradiation experiments originate from irradiation of the samples and not from a TPD heating to 300 K. The PI-ReTOF-MS data exhibit more complexity at a higher irradiation temperature (Figure 1, Supporting Information), which is detailed below.

3.1. $m/z = 34$ and 36

The signals from $m/z = 34$ and 36 can be assigned to H_2^{32}S ($\text{IE} = 10.453 \pm 0.008$ eV; Walters & Blais, 1984) and H_2^{34}S , respectively (Figure 2). First, we demonstrate the $m/z = 36$ signal is associated to isotopic species H_2^{34}S . While tricarbon (C_3 , $\text{IE} = 13.0 \pm 0.1$ eV; Ramanathan et al., 1993), hypofluorous acid ($\text{IE} = 12.69 \pm 0.03$ eV; Berkowitz et al., 1973), and hydrogen chloride ($\text{IE} = 12.752 \pm 0.006$ eV; Pennetreau et al., 1983) can match $m/z = 36$ in principal, their ionization energies are above the photon energy of 10.49 eV used in the experiment; hence, these molecules would not be detectable. Signal at $m/z = 36$ cannot be assigned to deuterated silane (SiD_4) and/or methanol (CD_3OD) because the nonisotopic signal at $m/z = 32$ for silane (SiH_4) and/or methanol (CH_3OH) is lacking. Second, the ratio (0.049 ± 0.005) of the integrated areas of signal at $m/z = 36$ and 34 agrees quite well with the natural abundance ratio of ^{34}S and ^{32}S (0.045; Cooper et al., 1997), which confirms the assignments of H_2^{34}S ($m/z = 36$) and H_2^{32}S ($m/z = 34$). The contribution of D_2^{32}S to the $m/z = 36$ is negligible due to low natural deuterium abundance of only 0.00015. Note that the sublimation temperature of H_2S in this study is higher than that of pure H_2S ice (Jiménez-Escobar & Muñoz Caro, 2011), which is likely due to the molecular interaction between H_2S and silicates.

3.2. $m/z = 64, 66$, and 68

The ion signals at $m/z = 64$, 66, and 68 can be assigned to $^{32}\text{S}_2$, $\text{H}_2^{32}\text{S}_2$ ($\text{IE} = 9.3$ eV; Wagner & Bock, 1974), and $\text{H}_2^{32}\text{S}^{34}\text{S}$, respectively. The ratio of integrated area of $m/z = 68$ and 66 is calculated to be 0.092 ± 0.009 , which is consistent with the natural abundance ratio of $\text{H}_2^{32}\text{S}_2$ and $\text{H}_2^{32}\text{S}^{34}\text{S}$ (0.089). The weak ion signal at $m/z = 64$ may be due to minor fragmentation of $\text{H}_2^{32}\text{S}_2$ rather than direct sublimation of S_2 from the sample (Jiménez-Escobar et al., 2012; Jiménez-Escobar & Muñoz Caro, 2011). The above mentioned signal at $m/z = 34$ (H_2S) cannot be linked to fragments of H_2S_2 since this signal is much more intense than $m/z = 66$ while our “soft” ionization method does not result in so major fragmentation (Abplanalp et al., 2015).

4. Discussion

Our results establish that the generation of H_2S and H_2S_2 via a simultaneous electron and laser irradiation of the Murchison meteorite occurs. Next, it is important to briefly discuss possible underlying formation mechanisms. Various sulfur-containing species such as pentlandite ($(\text{Fe},\text{Ni})_9\text{S}_8$), tochilinite (interlayered

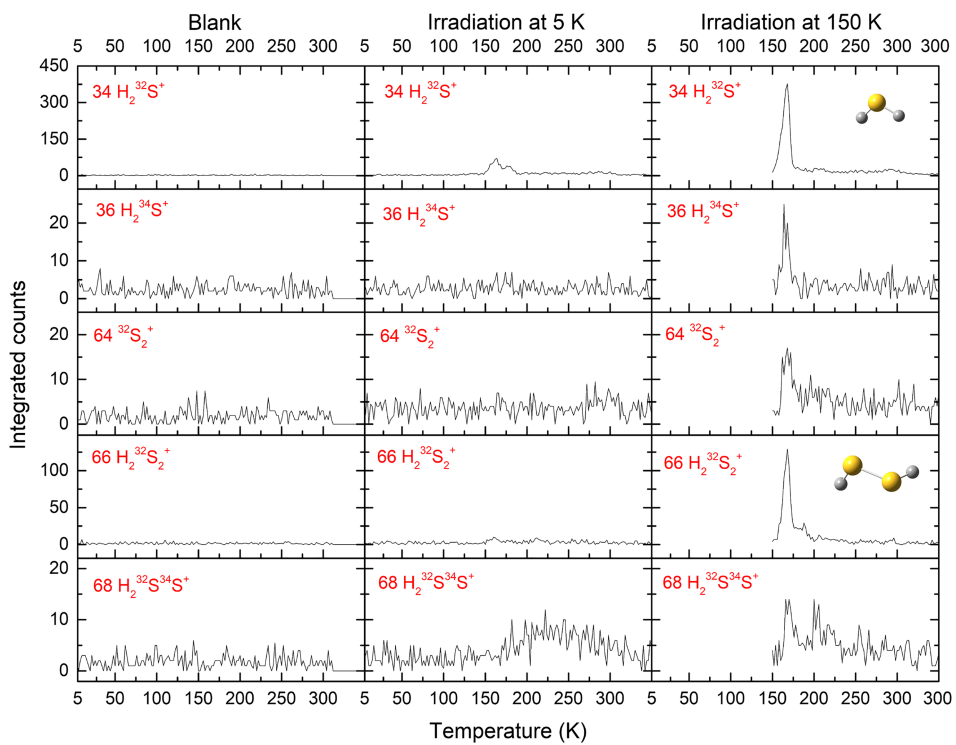


Figure 2. Temperature programmed desorption (TPD) profiles recorded via photoionization reflectron time-of-flight mass spectrometry (PI-ReTOF-MS) for $m/z = 34, 36, 64, 66$, and 68 . The weak $m/z = 64$ signal ($^{32}\text{S}_2^+$) is due to fragmentation of $\text{H}_2^{32}\text{S}_2^+$.

FeS and MgOH layers; Labidi et al., 2017), troilite (FeS; Levin et al., 2007), pyrrhotite ($\text{Fe}_{(1-x)}\text{S}$ ($x = 0$ – 0.2)); Palmer & Lauretta, 2011), Murchisite (Cr_5S_6 ; Ma et al., 2011), and alkyl sulfonic acids ($\text{CH}_3\text{SO}_3\text{H}$, $\text{C}_2\text{H}_5\text{SO}_3\text{H}$; Cooper et al., 1992) have been found in the Murchison meteorite. During the irradiation of the sample to typically $0.14 \mu\text{m}$ depth, the energetic electrons easily break weak chemical bonds like Fe-S and S-H, which have typical bond energies of only 3.51 and 3.76 eV, respectively; thus generating suprathermal sulfur and hydrogen atoms (Bennett et al., 2006). Since these atoms have excess kinetic energies, diffuse recombination reactions such as $\text{H} + \text{S} \rightarrow \text{HS}$, $\text{HS} + \text{H} \rightarrow \text{H}_2\text{S}$, and $\text{HS} + \text{HS} \rightarrow \text{H}_2\text{S}_2$ can proceed even at temperatures as low as 5.5 K. H_2S may also serve as a precursor to H_2S_2 . Previous laboratory experiments found that irradiation of H_2S ices led to the formation of H_2S_2 (Jiménez-Escobar et al., 2012; Jiménez-Escobar & Muñoz Caro, 2011). These newly formed species may be trapped in micropores and/or vesicles in the sample (Zhu et al., 2019) and therefore were not detected in preliminary experiments with only energetic electron irradiation. Once formed within the sample, the simulated micrometeorite impact likely induces thermal diffusion of the sulfur-bearing molecules to the surface, where they may sublime during the TPD phase. The irradiation at higher temperature of 150 K significantly enhances the thermal effects (diffusion) and therefore generates appreciably enhanced surface H_2S and H_2S_2 (Figure 2). Taken quantitatively, the high temperature irradiations generated more H_2S and H_2S_2 than the low temperature experiments by factors of 4.1 ± 0.5 and 10.5 ± 1.0 , respectively. The higher temperature experiments are more applicable to Bennu (230–280 K) and Ryugu (260–400 K). We predict with these even higher temperatures for the asteroids, that more H_2S and H_2S_2 is generated and that it is released instantaneously upon formation. Furthermore, the laser can also vibrationally excite the C-H and Fe-S stretches in the sample exposed to electrons. It has been reported that the bond rupture processes and reactions of vibrationally excited molecules are considerably enhanced compare to their counterpart in the vibrational ground state (Palma et al., 2002). This effect may enrich the energetic sulfur and hydrogen atoms in the sample and therefore produce more H_2S and H_2S_2 . Unlike the present results, Gillis-Davis et al. (2017) detected H_2S during solely laser irradiation of a chondrite. However, the previous experiments were performed at room temperature. Laser irradiation-induced thermal effect may

decompose the sulfur-containing molecules and generate surface H₂S at room temperature, while these thermal processes are much less efficient at low temperatures (5 and 150 K) and therefore electron irradiation is needed to generate detectable H₂S as well as H₂S₂.

5. Conclusion

The present study demonstrates the formation of H₂S and H₂S₂ upon simulated space weathering of the Murchison meteorite, which is performed via simultaneous exposure of the samples to energetic electrons and laser irradiation as proxies for interaction with charged particles from the solar wind as well as galactic cosmic rays and micrometeorite bombardment, respectively. These compounds are converted from the sulfur-containing minerals in the exposed samples. The Murchison meteorite is classified as a CM2 chondrite and is suggested to originate from C-type asteroids. The current C-complex asteroid sample-return missions Osiris-Rex/NASA (launched in 2016) and Hayabusa 2/JAXA (launched in 2014) have investigated asteroids 101955 Bennu and 162173 Ryugu, respectively, and will return samples from these objects. Our measurements of volatile H₂S and H₂S₂ generated via simulated space weathering of the Murchison meteorite implies that Osiris-Rex and Hayabusa 2 missions would detect low surficial sulfur abundance on asteroids 101955 Bennu and 162173 Ryugu, respectively, since space-weathering processes occur on these airless bodies. Furthermore, as H₂S and H₂S₂ will sublime when the samples from asteroids are allowed to reach temperatures higher than 150 K (Figure 2), and H₂S₂ is unstable at ambient temperatures on Earth, cryogenic curation of future samples from cold asteroids is necessary to keep scientific integrity of these fragile species (Calaway & Allen, 2011).

Acknowledgments

There are no conflicts to declare. All data used in this paper are available online as supporting information and can be accessed at <http://uhmreactiondynamics.org/publications.html>. This work was supported by NASA under grants NNX16AO79G (RIK) and NNX15AH58G (JJGD) to the University of Hawaii. We would also like to acknowledge the W.M. Keck Foundation to fund the construction of the surface science machine; Parker Crandall (UH Manoa, Department of Chemistry) provided advice to operate the laser.

References

- Abplanalp, M. J., Borsuk, A., Jones, B. M., & Kaiser, R. I. (2015). On the formation and isomer specific detection of propenal (C₂H₃CHO) and cyclopropanone (c-C₃H₄O) in interstellar model ices—A combined FTIR and reflectron time-of-flight mass spectroscopic study. *The Astrophysical Journal*, 814(1), 45. <https://doi.org/10.1088/0004-637X/814/1/45>
- Abplanalp, M. J., Förstel, M., & Kaiser, R. I. (2016). Exploiting single photon vacuum ultraviolet photoionization to unravel the synthesis of complex organic molecules in interstellar ices. *Chemical Physics Letters*, 644, 79–98. <https://doi.org/10.1016/j.cplett.2015.11.029>
- Abplanalp, M. J., Gozem, S., Krylov, A. I., Shingledecker, C. N., Herbst, E., & Kaiser, R. I. (2016). A study of interstellar aldehydes and enols as tracers of a cosmic ray-driven nonequilibrium synthesis of complex organic molecules. *Proceedings of the National Academy of Sciences*, 113(28), 7727–7732. <https://doi.org/10.1073/pnas.1604426113>
- Basilevsky, A. T., Yakovlev, O. I., Fisenko, A. V., Semjonova, L. F., Semenova, A. S., Barsukova, L. D., et al. (2000). Simulation of impact melting effect on spectral properties of Martian surface: Implications for polar deposits. *Geochemistry International*, 38(1), 390–403.
- Bennett, C. J., Jamieson, C. S., Osamura, Y., & Kaiser, R. I. (2005). A combined experimental and computational investigation on the synthesis of acetaldehyde [CH₃CHO (X¹A')] in interstellar ices. *The Astrophysical Journal*, 624(2), 1097–1115. <https://doi.org/10.1086/429119>
- Bennett, C. J., Jamieson, C. S., Osamura, Y., & Kaiser, R. I. (2006). Laboratory studies on the irradiation of methane in interstellar, cometary, and solar system ices. *The Astrophysical Journal*, 653(1), 792–811. <https://doi.org/10.1086/508561>
- Berkowitz, J., Dehmer, J. L., & Appelman, E. H. (1973). Photoelectron spectrum of hypofluorous acid, HOF. *Chemical Physics Letters*, 19(3), 334–336. [https://doi.org/10.1016/0009-2614\(73\)80372-0](https://doi.org/10.1016/0009-2614(73)80372-0)
- Boamah, M. D., Sullivan, K. K., Shulenberger, K. E., Soe, C. M., Jacob, L. M., Yhee, F. C., et al. (2014). Low-energy electron-induced chemistry of condensed methanol: Implications for the interstellar synthesis of prebiotic molecules. *Faraday Discussions*, 168, 249–266. <https://doi.org/10.1039/C3FD00158J>
- Boyer, M. C., Boamah, M. D., Sullivan, K. K., Arumainayagam, C. R., Bazin, M., Bass, A. D., & Sanche, L. (2014). Dynamics of dissociative electron–Molecule interactions in condensed methanol. *The Journal of Physical Chemistry C*, 118(39), 22,592–22,600. <https://doi.org/10.1021/jp506365d>
- Brunetto, R., Roush, T. L., Marra, A. C., & Orofino, V. (2007). Optical characterization of laser ablated silicates. *Icarus*, 191(1), 381–393. <https://doi.org/10.1016/j.icarus.2007.04.023>
- Burbine, T. H. (2014). Asteroids. In *Treatise on geochemistry*, (pp. 365–415). Oxford: Elsevier.
- Calaway, M. J., & Allen, C. C. (2011). Cold and cryogenic curation of lunar volatile samples returned to earth. Paper presented at A wet vs. dry moon: Exploring volatile reservoirs and implications for the evolution of the moon and future exploration, Lunar and Planetary Institute, Houston, Texas.
- Chapman, C. R. (1995). Near earth asteroid rendezvous: Eros as the key to the S-type conundrum. Paper presented at 26th lunar and planetary science conference, Lunar and Planetary Institute, Houston, Texas.
- Chapman, C. R., Paolicchi, P., Zappala, V., Binzel, R. P., & Bell, J. F. (1989). Asteroid families-Physical properties and evolution. Paper presented at Asteroids II.
- Cooper, G. W., Onwo, W. M., & Cronin, J. R. (1992). Alkyl phosphonic acids and sulfonic acids in the Murchison meteorite. *Geochimica et Cosmochimica Acta*, 56(11), 4109–4115. [https://doi.org/10.1016/0016-7037\(92\)90023-C](https://doi.org/10.1016/0016-7037(92)90023-C)
- Cooper, G. W., Thiemens, M. H., Jackson, T. L., & Chang, S. (1997). Sulfur and hydrogen isotope anomalies in meteorite sulfonic acids. *Science*, 277(5329), 1072–1074. <https://doi.org/10.1126/science.277.5329.1072>
- Crandall, P. B., Góbi, S., Gillis-Davis, J. J., & Kaiser, R. I. (2017). Can perchlorates be transformed to hydrogen peroxide (H₂O₂) products by cosmic rays on the Martian surface? *Journal of Geophysical Research: Planets*, 122, 1880–1892. <https://doi.org/10.1002/2017JE005329>
- DeMeo, F. E., & Carry, B. (2014). Solar System evolution from compositional mapping of the asteroid belt. *Nature*, 505(7485), 629–634. <https://doi.org/10.1038/nature12908>

- Drouin, D., Couture, A. R., Joly, D., Tastet, X., Aimez, V., & Gauvin, R. (2007). CASINO V2.42-A Fast and Easy-to-Use Modeling Tool for Scanning Electron Microscopy and Microanalysis Users. *Scanning*, (3), 92–101. <https://doi.org/10.1002/sca.20000>
- Fletcher, A., Close, S., & Mathias, D. (2015). Simulating plasma production from hypervelocity impacts. *Physics of Plasmas*, 22(9), 093504. <https://doi.org/10.1063/1.4930281>
- Foley, C. N., Nittler, L. R., McCoy, T. J., Lim, L. F., Brown, M. R. M., Starr, R. D., & Trombka, J. I. (2006). Minor element evidence that Asteroid 433 Eros is a space-weathered ordinary chondrite parent body. *Icarus*, 184(2), 338–343. <https://doi.org/10.1016/j.icarus.2006.05.011>
- Gillis-Davis, J. J., Lucey, P. G., Bradley, J. P., Ishii, H. A., Kaluna, H. M., Misra, A., & Connolly Jr., H. C. (2017). Incremental laser space weathering of Allende reveals non-lunar like space weathering effects. *Icarus*, 286, 1–14. <https://doi.org/10.1016/j.icarus.2016.12.031>
- Gillis-Davis, J. J., & Scott, E. R. D. (2014). Explaining the sulfur depletion on Eros and the different space weathering of S-type and V-type asteroids. Paper presented at 45th Lunar and Planetary Science Conference, Lunar and Planet. Inst., The Woodlands, Texas.
- Harris, T. D., Lee, D. H., Blumberg, M. Q., & Arumainayagam, C. R. (1995). Electron-induced reactions in methanol ultrathin films studied by temperature-programmed desorption: A useful method to study radiation chemistry. *The Journal of Physical Chemistry*, 99(23), 9530–9535. <https://doi.org/10.1021/j100023a035>
- Hiroi, T., Moroz, L. V., Shingareva, T. V., Basilevsky, A. T., & Pieters, C. M. (2003). Effects of microsecond pulse laser irradiation on Vis-NIR reflectance spectrum of carbonaceous chondrite simulant: Implications for martian moons and primitive asteroids. Paper presented at 34th Lunar and Planetary Science Conference, Lunar and Planetary Institute, League City, Texas.
- Hiroi, T., & Sasaki, S. (2001). Importance of space weathering simulation products in compositional modeling of asteroids: 349 Dembowska and 446 Aeternitas as examples. *Meteoritics & Planetary Science*, 36(12), 1587–1596. <https://doi.org/10.1111/j.1945-5100.2001.tb01850.x>
- Jiménez-Escobar, A., & Muñoz Caro, G. M. (2011). Sulfur depletion in dense clouds and circumstellar regions-I. H₂S ice abundance and UV-photochemical reactions in the H₂O-matrix. *Astronomy & Astrophysics*, 536, A91. <https://doi.org/10.1051/0004-6361/201014821>
- Jiménez-Escobar, A., Muñoz Caro, G. M., Ciaravella, A., Cecchi-Pestellini, C., Candia, R., & Micela, G. (2012). Soft X-Ray irradiation of H₂S ice and the presence of S₂ in comets. *The Astrophysical Journal Letters*, 751(2), L40. <https://doi.org/10.1088/2041-8205/751/2/L40>
- Johnson, R. E. (1990). *Energetic charged-particle interactions with atmospheres and surfaces*. Berlin Heidelberg: Springer-Verlag.
- Jones, B. M., & Kaiser, R. I. (2013). Application of reflectron time-of-flight mass spectroscopy in the analysis of astrophysically relevant ices exposed to ionization radiation: Methane (CH₄) and D₄-methane (CD₄) as a case study. *The Journal of Physical Chemistry Letters*, 4(11), 1965–1971. <https://doi.org/10.1021/jz400692r>
- Keller, L. P., & Berger, E. L. (2014). A transmission electron microscope study of Itokawa regolith grains. *Earth, Planets and Space*, 66(1), 71. <https://doi.org/10.1186/1880-5981-66-71>
- Keller, L. P., Rahman, Z., Hiroi, T., Sasaki, S., Noble, S. K., Horz, F., & Cintala, M.J. (2013). Asteroidal space weathering: The major role of FeS. Paper presented at 44th Lunar and Planetary Science Conference, Lunar and Planetary Institute, The Woodlands, Texas.
- Kelley, M. S., Gaffey, M. J., Vilas, F., & Hardersen, P. S. (2001). Recent, ground-based, near-infrared spectral observations of asteroid 433 Eros. Paper presented at 32nd Lunar and Planetary Science Conference, Lunar and Planetary Institute, Houston, Texas.
- Killen, R. M. (2003). Depletion of sulfur on the surface of asteroids and the Moon. *Meteoritics & Planetary Science*, 38(3), 383–388. <https://doi.org/10.1111/j.1945-5100.2003.tb00273.x>
- Kracher, A., & Sears, D. W. G. (2005). Space weathering and the low sulfur abundance of Eros. *Icarus*, 174(1), 36–45. <https://doi.org/10.1016/j.icarus.2004.10.010>
- Labidi, J., Farquhar, J., Alexander, C. M. O'D., Eldridge, D. L., & Oduro, H. (2017). Mass independent sulfur isotope signatures in CMs: Implications for sulfur chemistry in the early solar system. *Geochimica et Cosmochimica Acta*, 196, 326–350. <https://doi.org/10.1016/j.gca.2016.09.036>
- Levin, E. M., Bud'ko, S. L., Mao, J. D., Huang, Y., & Schmidt-Rohr, K. (2007). Effect of magnetic particles on NMR spectra of Murchison meteorite organic matter and a polymer-based model system. *Solid State Nuclear Magnetic Resonance*, 31(2), 63–71. <https://doi.org/10.1016/j.ssnmr.2007.01.002>
- Loeffler, M. J., Dukes, C. A., Chang, W. Y., McFadden, L. A., & Baragiola, R. A. (2008). Laboratory simulations of sulfur depletion at Eros. *Icarus*, 195(2), 622–629. <https://doi.org/10.1016/j.icarus.2008.02.002>
- Love, S. G., & Brownlee, D. (1993). A direct measurement of the terrestrial mass accretion rate of cosmic dust. *Science*, 262(5133), 550–553. <https://doi.org/10.1126/science.262.5133.550>
- Lucey, P., Korotev, R. L., Gillis, J. J., Taylor, L. A., Lawrence, D., Campbell, B. A., et al. (2006). Understanding the lunar surface and space-Moon interactions. *Reviews in Mineralogy and Geochemistry*, 60(1), 83–219. <https://doi.org/10.2138/rmg.2006.60.2>
- Ma, C., Beckett, J. R., & Rossman, G. R. (2011). Murchisite, Cr₅S₆, a new mineral from the Murchison meteorite. *American Mineralogist*, 96(11–12), 1905–1908. <https://doi.org/10.2138/am.2011.3858>
- McCausland, P. J. A., Samson, C., & McLeod, T. (2011). Determination of bulk density for small meteorite fragments via visible light 3-D laser imaging. *Meteoritics & Planetary Science*, 46(8), 1097–1109. <https://doi.org/10.1111/j.1945-5100.2011.01217.x>
- McCoy, T. J., Burbine, T. H., McFadden, L. A., Starr, R. D., Gaffey, M. J., Nittler, L. R., et al. (2001). The composition of 433 Eros: A mineralogical-chemical synthesis. *Meteoritics & Planetary Science*, 36(12), 1661–1672. <https://doi.org/10.1111/j.1945-5100.2001.tb01855.x>
- McFadden, L. A., Wellnitz, D. D., Schnaubelt, M., Gaffey, M. J., Bell III, J. F., Izenberg, N., et al. (2001). Mineralogical interpretation of reflectance spectra of Eros from NEAR near-infrared spectrometer low phase flyby. *Meteoritics & Planetary Science*, 36(12), 1711–1726. <https://doi.org/10.1111/j.1945-5100.2001.tb01858.x>
- Moroz, L. V., Basilevsky, A. T., Hiroi, T., Rout, S. S., Baither, D., van der Bogert, C. H., et al. (2009). Spectral properties of simulated impact glasses produced from martian soil analogue JSC Mars-1. *Icarus*, 202(1), 336–353. <https://doi.org/10.1016/j.icarus.2009.02.007>
- Moroz, L. V., Fisenko, A. V., Semjonova, L. F., Pieters, C. M., & Korotaeva, N. N. (1996). Optical effects of regolith processes on S-asteroids as simulated by laser shots on ordinary chondrite and other mafic materials. *Icarus*, 122(2), 366–382. <https://doi.org/10.1006/icar.1996.0130>
- Moroz, L. V., Hiroi, T., Shingareva, T. V., Basilevsky, A. T., Fisenko, A. V., Semjonova, L. F., & Pieters, C. M. (2004). Reflectance spectra of CM2 chondrite Mighei irradiated with pulsed laser and implications for low-albedo asteroids and Martian moons. Paper presented at 35th Lunar and Planetary Science Conference, Lunar and Planetary Institute, League City, Texas.
- Murchie, S. L., & Pieters, C. M. (1996). Spectral properties and rotational spectral heterogeneity of 433 Eros. *Journal of Geophysical Research*, 101(E1), 2201–2214. <https://doi.org/10.1029/95JE03438>
- Nittler, L. R., Starr, R. D., Lim, L., McCoy, T. J., Burbine, T. H., Reedy, R. C., et al. (2001). X-ray fluorescence measurements of the surface elemental composition of asteroid 433 Eros. *Meteoritics & Planetary Science*, 36(12), 1673–1695. <https://doi.org/10.1111/j.1945-5100.2001.tb01856.x>
- Palma, J., Echave, J., & Clary, D. C. (2002). The effect of the symmetric and asymmetric stretching vibrations on the CH₃D + O(³P) → CH₃ + OD reaction. *Chemical Physics Letters*, 363(5–6), 529–533. [https://doi.org/10.1016/S0009-2614\(02\)01239-3](https://doi.org/10.1016/S0009-2614(02)01239-3)

- Palmer, E. E., & Lauretta, D. S. (2011). Aqueous alteration of kamacite in CM chondrites. *Meteoritics & Planetary Science*, 46(10), 1587–1607. <https://doi.org/10.1111/j.1945-5100.2011.01251.x>
- Pennetreau, P., Natalis, P., Longton, L., & Collin, J. (1983). Ionization energies for the vibronic transitions from DCI $X^1\Sigma^+(v'' = 0)$ to DCI $+X^2\Pi(v' = 0 - 18)$ and $A^3\Sigma^+(v' = 0 - 17)$ determined by photoelectron spectroscopy. *Journal of Electron Spectroscopy and Related Phenomena*, 28(3), 295–297. [https://doi.org/10.1016/0368-2048\(83\)80008-5](https://doi.org/10.1016/0368-2048(83)80008-5)
- Ramanathan, R., Zimmerman, J. A., & Eyler, J. R. (1993). Ionization potentials of small carbon clusters. *The Journal of Chemical Physics*, 98(10), 7838–7845. <https://doi.org/10.1063/1.464591>
- Sasaki, S., Nakamura, K., Hamabe, Y., Kurahashi, E., & Hiroi, T. (2001). Production of iron nanoparticles by laser irradiation in a simulation of lunar-like space weathering. *Nature*, 410(6828), 555–557. <https://doi.org/10.1038/35069013>
- Shingareva, T. V., Basilevsky, A. T., Fisenko, A. V., Semjonova, L. F., & Korotaeva, N. N. (2004). Mineralogy and petrology of laser irradiated carbonaceous chondrite Mighei. Paper presented at 35th Lunar and Planetary Science Conference, Lunar and Planetary Institute, League City, Texas.
- Shingledecker, C. N., & Herbst, E. (2018). A general method for the inclusion of radiation chemistry in astrochemical models. *Physical Chemistry Chemical Physics*, 20(8), 5359–5367. <https://doi.org/10.1039/C7CP05901A>
- Strazzulla, G., & Johnson, R. E. (1989). Irradiation effects on comets and cometary debris. Paper presented at International Astronomical Union Colloquium, Cambridge University Press.
- Trombka, J. I., Squyres, S. W., Brückner, J., Boynton, W. V., Reedy, R. C., McCoy, T. J., et al. (2000). The elemental composition of asteroid 433 Eros: Results of the NEAR-Shoemaker X-ray spectrometer. *Science*, 289(5487), 2101–2105. <https://doi.org/10.1126/science.289.5487.2101>
- Turner, A. M., Abplanalp, M. J., Chen, S. Y., Chen, Y. T., Chang, A. H., & Kaiser, R. I. (2015). A photoionization mass spectroscopic study on the formation of phosphanes in low temperature phosphine ices. *Physical Chemistry Chemical Physics*, 17(41), 27,281–27,291. <https://doi.org/10.1039/C5CP02835C>
- Turner, A. M., Abplanalp, M. J., & Kaiser, R. I. (2016). Mechanistic studies on the radiolytic decomposition of perchlorates on the Martian surface. *The Astrophysical Journal*, 820(2), 127. <https://doi.org/10.3847/0004-637X/820/2/127>
- Turner, A. M., Bergantini, A., Abplanalp, M. J., Zhu, C., Góbi, S., Sun, B.-J., et al. (2018). An interstellar synthesis of phosphorus oxoacids. *Nature Communications*, 9(1), 3851. <https://doi.org/10.1038/s41467-018-06415-7>
- Wagner, G., & Bock, H. (1974). Photoelektronenspektren und molekülleigenschaften, XXVI. Die delokalisation von Schwefel-Elektronenpaaren in alkylsulfiden und-disulfiden. *European Journal of Inorganic Chemistry*, 107(1), 68–77. <https://doi.org/10.1002/cber.19741070109>
- Walters, E., & Blais, N. C. (1984). Molecular beam photoionization and fragmentation of D_2S , $(H_2S)_2$, $(D_2S)_2$, and H_2S-H_2O . *The Journal of Chemical Physics*, 80(7), 3501–3502. <https://doi.org/10.1063/1.447110>
- Wasson, J. T., Pieters, C. M., Fisenko, A. V., Semjonova, L. F., & Warren, P. H. (1998). Simulation of space weathering of eucrites by laser impulse irradiation. Paper presented at 29th Lunar and Planetary Science Conference, Lunar and Planetary Institute, Houston, Texas.
- Zhu, C., Crandall, P. B., Gillis-Davis, J. J., Ishii, H. A., Bradley, J. P., Corley, L. M., & Kaiser, R. I. (2019). Untangling the formation and liberation of water in the lunar regolith. *Proceedings of the National Academy of Sciences*, 116(23), 11,165–11,170. <https://doi.org/10.1073/pnas.1819600116>
- Zook, H. A., Flaherty, R. E., & Kessler, D. J. (1970). Meteoroid impacts on the Gemini windows. *Planetary and Space Science*, 18(7), 953–964. [https://doi.org/10.1016/0032-0633\(70\)90099-1](https://doi.org/10.1016/0032-0633(70)90099-1)